ISSN 2176-5480

22nd International Congress of Mechanical Engineering (COBEM 2013)
November 3-7, 2013, Ribeirão Preto, SP, Brazil

WALL CORRECTION FOR A NACA 0012 IN A SMALL SUBSONIC INDUCTION DRIVEN WIND TUNNEL WITH THE AID OF NUMERICAL CALCULATION

João Batista Pessoa Falcão Filho
IAE – Institute of Aeronautics and Space, Pça. Marechal Eduardo Gomes, 50, São José dos Campos – SP, CEP 12.228-904
jb.falcao@ig.com.br

Ariane Fassina Bredariol
UNITAU – Universidade de Taubaté, Rua Daniel Danelli, s/n, Jardim Morumbi, Taubaté – SP, CEP 12060-440
aribreda@hotmail.com

Abstract. *A small induction driven wind tunnel with cross-sectional area 0.144 m x 0.144 m was built in the Aerodynamic Division (ALA) of the Institute of Aeronautics and Space (IAE) to be used as a useful tool in subsonic aerodynamic academic tests. After many functional tests, a two-dimensional model of a NACA 0012 profile was installed to assess the reliability characteristics of the tunnel in performing tests of real interest, by means of pressure distribution over the profile. The focus is to study the influence of the wind tunnel solid walls, which are of great importance in case of subsonic test sections. Particularly, the problem represents a real challenge since the available model has 7% of blockage area ratio, which is relatively high for typical subsonic wind tunnel tests. In a first attempt theoretical and empirical approaches from the specialized literature were used to reasonably correct the pressure coefficient distribution. Now, numerical simulation is carried out to help with the wall corrections extrapolations. Euler equations approach were used to simulate the test section region installed with the NACA 0012 profile, and the boundary layer was accounted for by modifying the solid walls geometry to comply with the theoretical prediction.*

Keywords: *Subsonic wind tunnel, NACA 0012, Wall correction, Numerical simulation, CFD*

1. INTRODUCTION

In some aspects, wind tunnels are simple installations that are used to experimentally assess aerodynamic behavior of an article under tests. However each tunnel has many particularities that distinguish one from another, even considering facilities with the same design. In other words, it is practically impossible to construct two identical wind tunnel installations. For this reason just after the shakedown phase a relatively long period of tests are undertaken during the so called calibration phase. Two types of tests are generally developed during the calibration process of a wind tunnel. First the facility is loaded up to its design limits in order to confirm the full extent of its operational envelope. Later the attention is given to the test section region were the test article would be installed: through many tests the installation is assessed to determine its flow characteristics. A low-speed steady airstream is usually considered to be defined by knowing its distribution of temperature, pressure, dynamic pressure and turbulence level (Barlow *et al.*, 1999). Various devices are used to better investigate the flow characteristics, such as Pitot tubes, pressure and temperature probes, hot-wire, yaw-meter probe, and also some specially designed devices for the particular installation. Finally some well known models are installed in the test section to verify the tunnel reliability by comparing the experimental results with results from other tunnels or from the literature. Among them the symmetrical profile NACA 0012 is greatly used as its experimental results are widely reported in the literature.

The Aerodynamic Division (ALA) from the Institute of Aeronautics and Space (IAE) has developed a small subsonic wind tunnel driven by injector, reaching in its test section Mach number 0.37. In Fig. 1 one can see the tunnel installation with the main components highlighted, namely: (1) the collector with geometry change, from circular to square, with area ratio of 5.4 and length of 0.305 m, (2) the squared test section with 0.144 m of side and 0.50 m of length, and with 3 windows for flow visualization; (3) one injector with fixed geometry operating in a chocked condition with Mach number 1.9 at its exit of 0.023 m x 0.016 m, and specially designed to be attached to the supply tubing; (4) the supersonic/subsonic mixing chamber with width of 0.173 m, height of 0.228 m and length of 0.685 m; (5) the diffuser with length of 1.725 m, and with superior and inferior articulated walls to allow angle adjustments from 0.8º to 8º; (6) the supply tubing with a pressure tap to measure the injector line stagnation pressure, which connects the supply air compressed system to the small tunnel circuit; (7) the traverse device to positioning pressure probes into the tunnel circuit.

The small tunnel utilizes air from the Injection System of the Pilot Transonic Wind Tunnel (TTP). For the sake of conciseness details of the TTP and the Injection System will not be presented herein but the interested reader can find them in Goffert *et al.* (2008).

ISSN 2176-5480

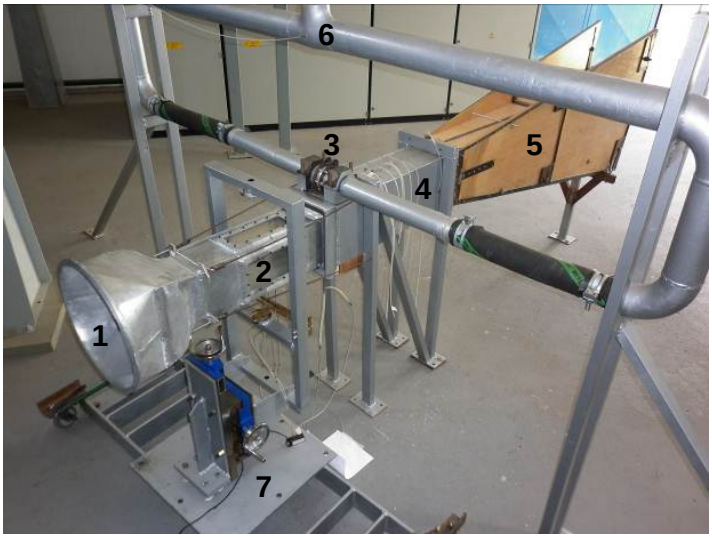

Figure 1. View of the installation of the small tunnel of ALA

Figure 2 shows a functional scheme of the small induction subsonic wind tunnel installation, highlighting its main cross sections. Compressed air is hold in reservoirs and during the tunnel operation it passes through a pressure control valve which modulates the injector stagnation pressure at stable desirable values from 2 to 12 bars. The high speed air flow delivered at the injector exit (1) creates low pressure environment in the mixing chamber inducing the main stream flow admitted from the atmosphere (2). If the pressure at the injectors is increased more mass flow is delivered by the injector and more air is admitted from the atmosphere, resulting in an increase of the main stream velocity. Both currents of the inductor and induced gases are subjected to a mixing process in the mixing chamber and finally a diffuser decelerates the flow to deliver it back to the atmosphere. The same induction principle can be found in many engineering applications, whenever small gas mass flow at high enthalpy is available and one needs to accelerate great amount of gas at relatively low enthalpy, for example, in aeronautical engines and in natural gas extraction process (Silva *et al.*, 2011).

In wind tunnel a special attention must be given to the flow quality in the test section region, where the model is to be installed. In most cases, provided that the inlet elements of the circuit are well designed a reasonably uniform velocity profile will be noticed in the test section. The small wind tunnel operates at atmospheric inlet condition, reaching Mach number from 0.1 to 0.37 in the test section, corresponding to Reynolds numbers variation from 60,000 to 210,000, considering a typical chord of 28.8 mm. More information about the tunnel design, for example the design of the injector, the design of the diffuser, the preliminary tests undertaken with the mixing chamber etc., can be found in Silva *et al.* (2010a, 2010b) and Faria (2011).

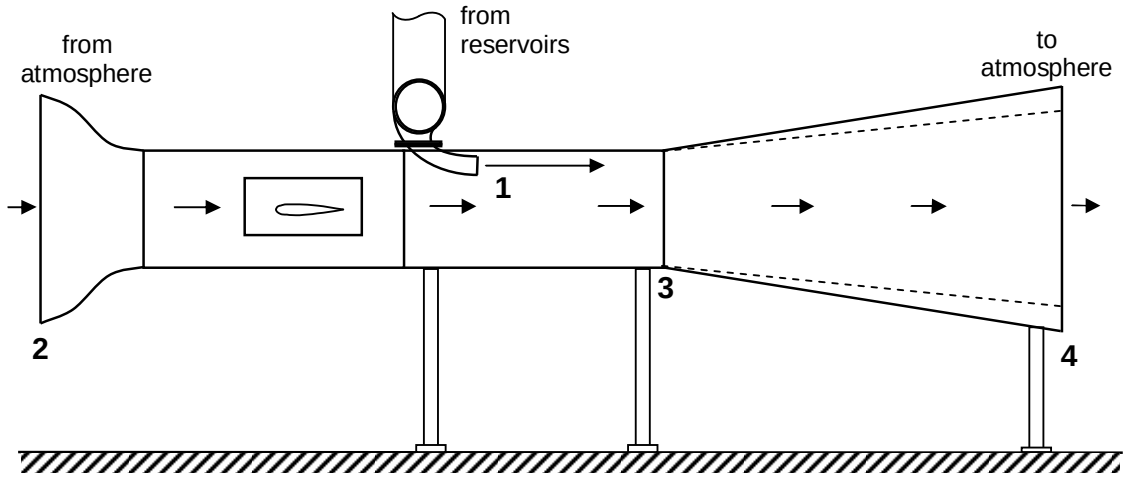

Figure 2. Scheme of the induction tunnel aerodynamic circuit

ISSN 2176-5480

After many tests undertaken in the small wind tunnel to investigate the uniformity and stability in the test section to better mimic the flight conditions, the tunnel was finally installed with a typical aerodynamic profile model, the NACA 0012, because of its vast literature that reports theoretical, numeric and experimental results in several wind tunnels and at several speed regimes. The profile NACA 0012 was developed in 1932 by NACA ("National Advisory Committee for Aeronautics") with a series known as NACA 4 digits. The numeration system to these airfoils is based on its geometry. The first digit indicates the maximum value of the ordinate y from the midline in percentage of the chord; the second digit is the distance from the leading edge to the maximum point of camber in tenths of the chord. The two final digits indicate the thickness of the airfoil in percentage of the chord. The NACA 0012 profile is symmetric, with maximum thickness of 12% in relation to the chord, and it can be expressed by the equation (Menezes, 1994)

$$\frac{y}{c} = \frac{t}{c}\left[a_0\sqrt{\frac{x}{c}} + a_1\left(\frac{x}{c}\right) + a_2\left(\frac{x}{c}\right)^2 + a_3\left(\frac{x}{c}\right)^3 + a_4\left(\frac{x}{c}\right)^4 \right] \tag{1}$$

where t is the maximum thickness, c is the chord and the constants are: a_0= 1.4779155, a_1= – 0.624424, a_2= 1.727016, a_3= 1.3840870 and a_4 = – 0.489769.

The profile utilized in the experiments was made out of Aluminum and machined in CNC to obtain a perfect representation of its geometry. The profile available with 7% of blockage ratio related to the test section dimensions was installed in horizontal direction into the test section (see Fig. 3 (a)). Five pressure taps of diameter 0.5 mm were perpendicularly drilled on the profile surface. The five pressure taps are located at 6%, 25.2%, 39.7%, 56.2% and 70.5% of the profile chord.

These pressure tap holes are connected to other holes of diameter 3 mm drilled laterally in the span-wise direction. Finally another hole of diameter 2 mm is made close to the extremity of the profile to meet the 3 mm hole (see Fig. 3(b)). The 3 mm hole has its extremity permanently closed with glue and the 2 mm hole receives a capillary tube which is fixed with glue and is connected by means of a long silicon hose to a pressure scanner (see Fig. 3 (b) and (c)) from the Pressure Systems Instruments (PSI, 2000). The pressure taps were located in only one side of the profile. So, as the profile NACA 0012 is symmetric, to obtain the pressure distribution in the lower and upper surfaces, with the profile at a determined angle of attack, the profile must be turned at the same angle in the other direction, to have the results in the other side. However in this work only the angle of attack zero was considered.

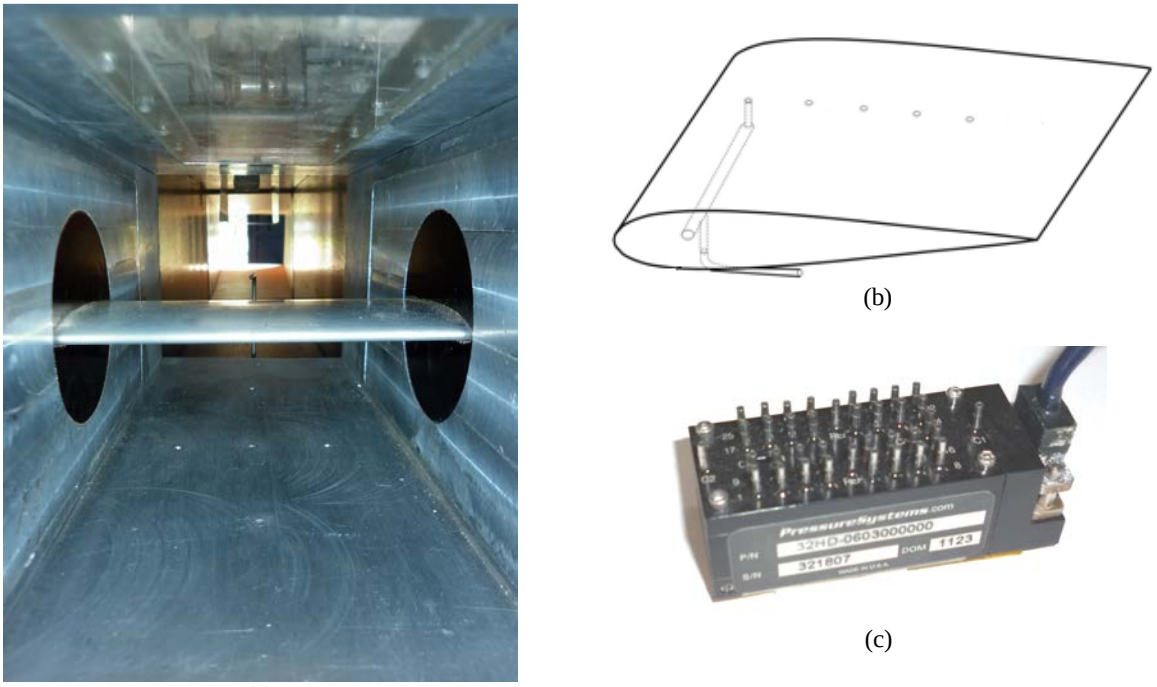

(a) (b) (c)

Figure 3. The NACA 0012 profile horizontally installed in the test section (a); scheme of the five pressure taps drilled on the profile surface with outside connections (b); pressure scanner with 32 channels from Pressure Systems Instruments (PSI, 2000) used in the tests

ISSN 2176-5480

The profile has 10 mm of thickness, with a blockage ratio of 7% – the blockage ratio is the ratio between the maximum cross-sectional area of the model and the test section cross-sectional area. With this relatively high blockage ratio for a solid wall test section it is expected that the obtained data need some kind of correction. This fact was treated in Bredariol *et al.* (2012), where the obtained pressure distribution results were corrected by consulting the literature. However the points closer to the trailing edge still presented strong discrepancies. So a more sophisticated correction procedure based on numerical calculation over the whole test section field is now envisaged by the present work.

2. WALL CORRECTION

Every object confined to be tested in a wind tunnel is under the action of several factors. Among them, one with most impact is the presence of the tunnel walls that can change the results if compared to a flow in a free flight. Wind tunnels with solid walls always will provoke an acceleration of the flow in the region where the article is installed, and so, the local measured pressure will be lower than that from real flight condition, where no solid frontiers exist. Modeling the whole test section installed with the NACA 0012 can be useful to determine the pressure decrease at each measuring point and to correct the local pressure value. Each local will have a different correction, depending on the numerical simulation results. For example, Fig. 4 shows two different situations concerning the same test article under flow condition. In the first situation (a) the article is at free flight with undisturbed pressure level p_∞ far upstream and at some distance upward and downward of it. In the second situation (b) the article is installed into the test section with the same undisturbed pressure level p_∞ considered at the test section entrance. In each case, at a determined local point over the model surface, the measured pressure values are p_1 and p_2. So, by knowing the pressure difference obtained in a numerical simulation ($p_1 - p_2$), the experimental measured local pressure p_m can be corrected for the wall effect using Eq. (2).

$$p_c = p_m - (p_1 - p_2). \tag{2}$$

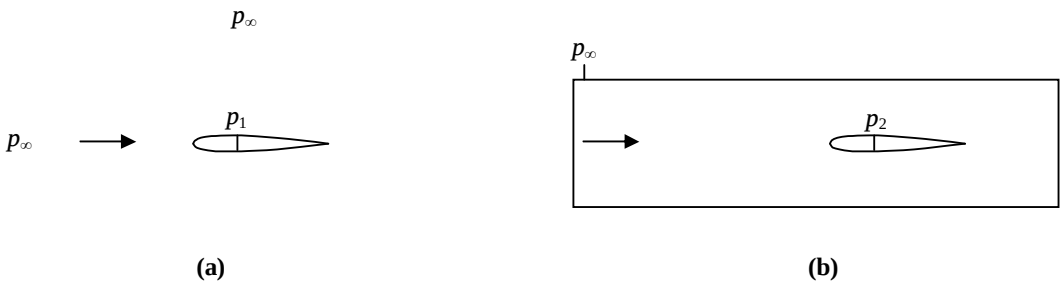

Figure 4. Two situations around the test article: (a) at free flight; (b) inside the tunnel test section

Since the pressure level is a dimensional quantity and may be different from each situation, a useful parameter commonly used to be corrected and also to be compared between distinct situations is the pressure coefficient, defined by (Anderson, 2007)

$$C_p \equiv \frac{p - p_\infty}{q_\infty}, \tag{3}$$

where p is the local pressure, p_∞ is the undisturbed pressure (far field) and q_∞ is the undisturbed dynamic pressure, defined by

$$q_\infty \equiv \frac{1}{2} \rho_\infty V_\infty^2, \tag{4}$$

where ρ_∞ is the undisturbed density and V_∞ is the undisturbed velocity. By combining Eqs. (3) and (4) with the perfect gas state equation ($p = \rho R T$) and the speed of sound expression ($a = \sqrt{\gamma R T}$), where R is the perfect gas constant and

ISSN 2176-5480

γ is the ratio of specific heat at constant pressure to that at constant volume, the pressure coefficient may be expressed more conveniently by

$$C_p = \frac{\frac{p}{p_\infty} - 1}{\frac{\gamma}{2} M_\infty^2}. \tag{5}$$

3. NUMERICAL SIMULATION

The numerical simulation proposed is based on a code developed to solve the Euler Equations in two-dimensional field by finite difference approach. By its characteristics the code has low computational cost being possible to give fast results with a reasonable computational mesh. A thorough investigation of the problem would necessarily point to a three-dimensional approach, since the lateral walls of the tunnel will also affect the flow distribution in the test section. But this will be the theme for a further analysis, as the present work is a preliminary approach to the problem.

Nevertheless the main point to be addressed here is how can it account for the boundary layer along the model surface, and particularly, along the tunnel wall. The boundary layer plays a very important role in the confined flow condition, where it can greatly contribute in accelerating the flow and, consequently, in lowering the local pressure.

So, a simplified turbulent model for the boundary-layer displacement-thickness growth along the tunnel wall was considered, based on Eqs. (21.6) and (21.8) from Schlichting (1979), and used as it is described by Eq. (6). In this situation x is the stream-wise distance measured from the test section entrance. Since the Reynolds number at the local where the model is installed (about 0.33 m) for the study case analyzed is of 1.3 million, the turbulent model adopted is a reasonable choice. In Eq. (6) is the cinematic viscosity and U_∞ is the undisturbed speed.

$$(x) = 0.04625\, x \left(\frac{}{U_\infty\, x} \right)^{0.2}. \tag{6}$$

On the other hand, over the model surface the turbulent model consideration is not perfectly adequate, since the Reynolds number related to the profile chord for the study case analyzed is about 330,000 and most of the profile region would probably be laminar. So, the laminar model for the boundary-layer displacement-thickness growth along the profile surface, based on Eq. (7.37) from Schlichting (1979), was used as it is described in Eq. (7), with the same definitions applied in Eq. (6).

$$(x) = 1.7208 \sqrt{\frac{x}{U_\infty}}. \tag{7}$$

The mathematical model is represented by the Euler Equations, written in generalized coordinates and conservation-law form. The medium is air considered as an isotropic and Newtonian fluid, and as a thermally and calorically perfect gas. The numerical algorithm follows closely the main lines of the finite-difference, implicit diagonal scheme due to Pulliam and Chaussee (1981), complemented by a non-linear, spectral-radius-based artificial dissipation strategy due to Pulliam (1986). The code is a simplified version of the code used in Falcão Filho and Ortega (2008).

Three meshes were considered for the study case simulations. Since the NACA 0012 profile is symmetric, in all three meshes the computational field was conceived considering the half physical field being imposed symmetrical conditions in the inferior interface, as it can be seen in Fig. 5. The flow direction in figure is from the left to the right. The same dimensions were applied in all cases in the lower frontier as they are presented in Fig. 5 (b). The idea was represent the physical condition of the profile with a chord of 0.083 m installed in the test section of the tunnel with total length of 0.50 m.

In the first case (Fig. 5 (a)) the mesh represents the conditions without the influence of the upper wall, having extended the upper frontier of the mesh from 0.072 m to 0.30 m and imposing far field condition at it. In the second case (Fig. 5 (b)) the upper wall proximity, as found in the tunnel installation, was represented by being imposed solid wall with slipping condition. The third case (Fig. 5 (c)) is the same as in the Fig. 5 (b) but now considering the displacement-thickness boundary-layer over the upper wall and over the profile surface, *i. e.*, the real mesh in this case was modified to give the correct limits to the "potential-like" flow.

In all cases symmetrical condition was imposed at the inferior frontier (except on the line which defines the profile geometry). In the inlet frontier stagnation condition was imposed and the speed was extrapolated from inside of the mesh, correctly representing the characteristic conditions for subsonic flow. In the outlet frontier all conditions were extrapolated except the pressure which was imposed, correctly representing the characteristic conditions for subsonic flow at the exit. This was, by adjusting the pressure at the exit frontier the numerical solution develops to a desirable

ISSN 2176-5480

flow condition at the entrance of the test section, mimicking the physics of the induction operation of the tunnel from atmospheric environment.

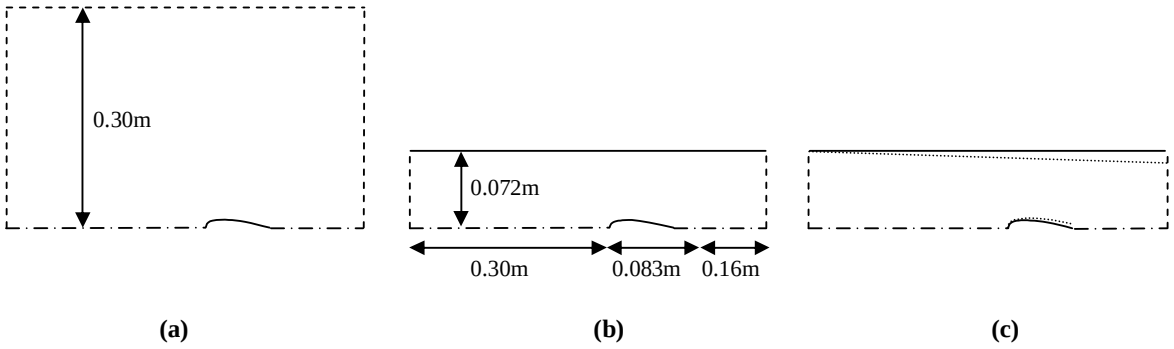

Figure 5. The three meshes of the half physical field considered for the study case simulations: (a) model in a free flight condition; (b) model installed in the test section; (c) model installed in the test section with the boundary-layer displacement-thickness growth

Figure 6 shows the mesh for the case represented in Fig. 5 (b) with 390 × 95 points, where it can be seen the node-clustering regions near the superior and inferior frontiers with the aim of better representing the boundary condition extrapolations – the minimum vertical displacement Δy_{min} in these regions was 6×10^{-5} m. The same number of points was used for the other cases – in the first case (Fig. 5 (a)), where the node-clustering was not needed in the upper frontier, the points were relocated giving place to a greater extent of the mesh in the upper direction.

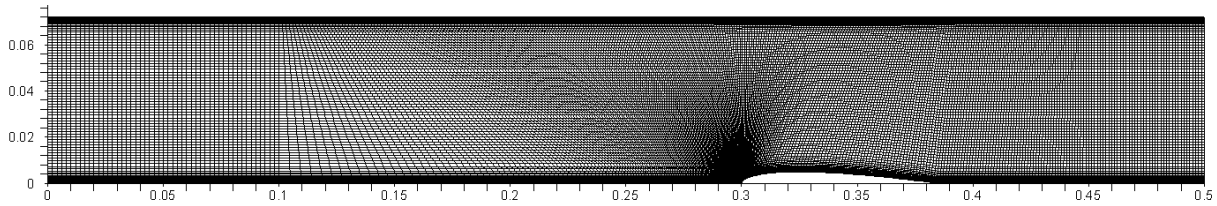

Figure 6. Mesh for the second case according to Fig. 5 (b), with 390 × 95 points

Figure 7 shows a closer view of the profile region for the second and the third cases represented by Fig. 5 (b) and (c), with the profile surface being represented by 95 grid points. In Fig. 7 (b) it is possible to note the laminar boundary-layer displacement-thickness growth indicated by the little kink in the mesh at the trailing edge (b) – the displacement-thickness at the trailing edge was 2.4×10^{-4} m.

The adjustment at the end of the profile because of the laminar boundary layer thickness in some way simulates the real physics as it creates a more precise environmental felt by the outer flow (outside the boundary layer): an abrupt interruption of the profile more accentuated than in the case of a thin profile end. A better result could only be possible by solving the Navier-Stokes equations, that will be consider for further research.

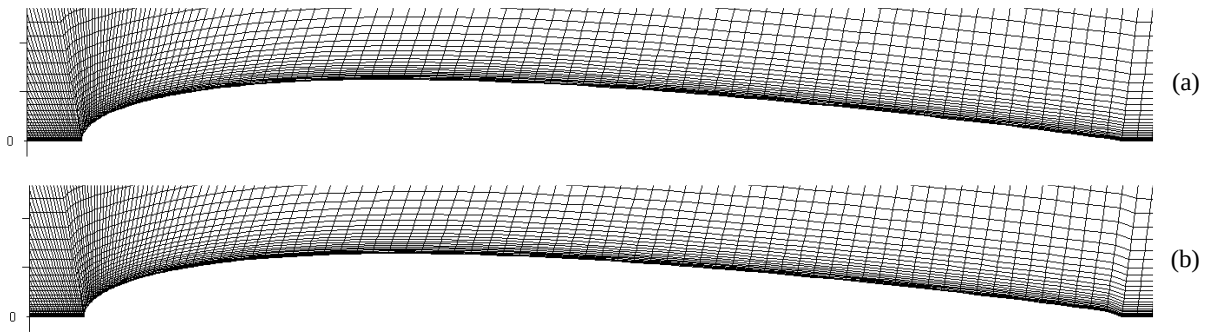

Figure 7. Close view of the profile surface for (a) second case (Fig. 5 (b)) and (b) third case (Fig. 5 (c))

ISSN 2176-5480

Figure 8 shows a closer view of the profile leading edge where one can se how well discretized and smooth are the the region with node-clustering in longitudinal direction chosen to better define the profile surface, and in the transversal direction to improve extrapolations close to solid walls. Observe that the transversal lines of the grid were chosen in such a direction to avoid null cells at the leading edge proximity and also to diminishing mesh stiffness.

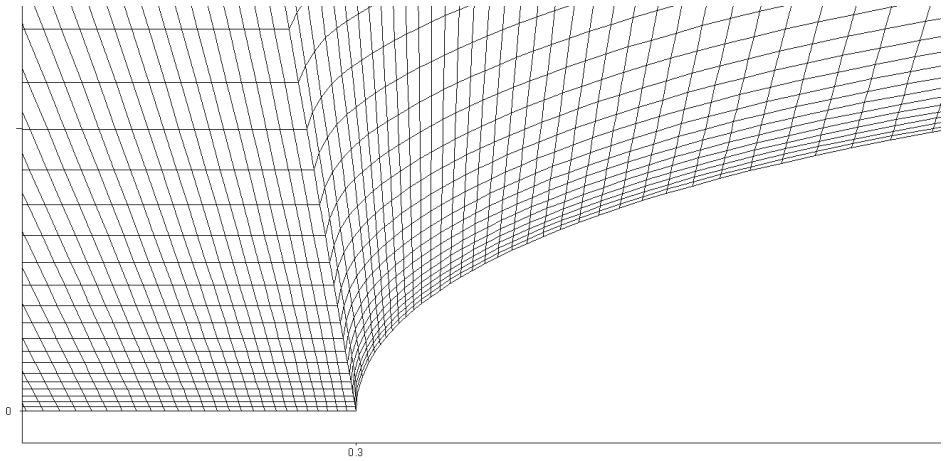

Figure 8. Close view of the profile leading edge region

4. RESULTS

Table 1 describes the experimental operating conditions of the tunnel installation considered in the present work. The tunnel was operated in the whole envelope up to Mach number 0.35, however for the sake of brevity only one typical operating configuration was selected to describe the used methodology of wall correction.

The operating conditions were imposed in the three numerical cases considered in Fig. 5: (1) free-flight condition; (2) test section without considering boundary-layer effects; (3) test section considering boundary-layer effects: turbulent flow on the tunnel wall and laminar flow on the profile surface.

Ambient conditions (temperature and pressure) were imposed in the numerical simulations at the inlet section as total flow properties – the atmospheric environment acts like a reservoir supplying the necessary mass flow which is inducted by the tunnel's injector.

Table 1. Operational conditions for the case study tested in the small wind tunnel (with temporal standard deviation)

Parameter	Value
Injector stagnation pressure (bar)	(4.01 ± 0.03) bar
Test section inlet Mach number	(0.181 ± 0.003)
Atmospheric temperature (C)	(23.4 ± 0.1) ^{o}C
Atmospheric pressure (Pa)	(94,090 ± 15) Pa

Figure 9 shows previous experiment results obtained in order to assure the flow quality in the small tunnel test section. In this experience, three Pitot probes were installed and they could travel vertically at a certain longitudinal station of the test section, in the region where the model would be installed. The test section was empty and the three probes could move through three holes in the floor of the test section: one at the center of the test section (2) and two at the middle distance between the center and the lateral walls (1 and 3). The three probes were fixed in a traverse system outside the test section in such a way that they could be positioned at a determined distance from the floor of the test section.

Mach number was evaluated based on local static and total pressure measurements obtained with the Pitot probes connected to pressure sensors. It is possible to observe a little decrease in the Mach number value as the three probes progress upward the test section cross section due to the blockage created by them. The spatial averaged Mach number read with the three probes in all positions was 0.1910 and the standard deviation was 0.0017, a very good result for an injector driven induction wind tunnel.

ISSN 2176-5480

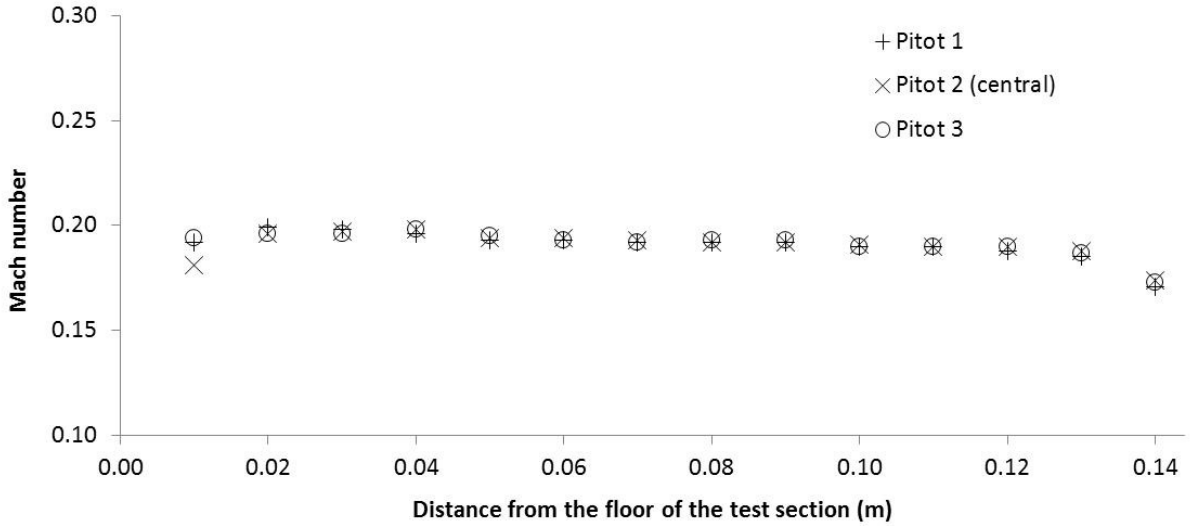

Figure 9. Mach number distribution in three vertical lines at a certain longitudinal station of the test section

Figure 10 shows the fields of Mach number (a) and pressure (b) for the third numerical simulation case study (considering the boundary-layer displacement-thickness over the solid frontiers). The presence of the boundary layer is observed in the upper wall and over the profile surface. It is possible to observe in the figure the slight negative slope in the upper frontier indicating the boundary-layer blockage presence along the wall. As expected, the region on the wall in the proximity of the profile feels its influence, and so, it endorses the need of some wall correction procedure. The results also indicate that the length of the test section is large enough, with an initial region for flow adjustment.

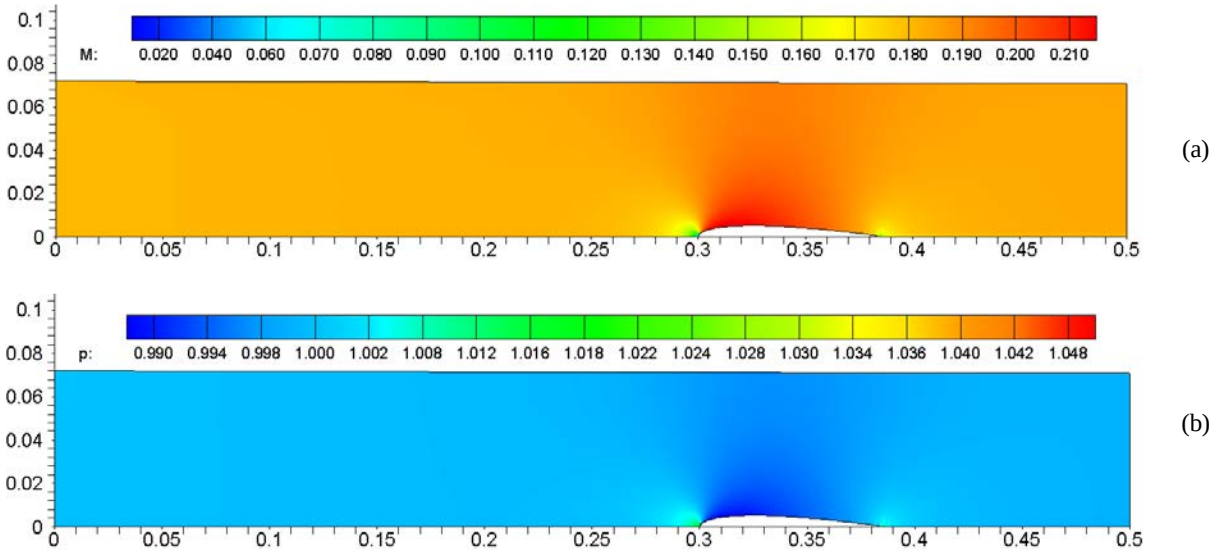

Figure 10. Mach number and pressure fields in the test section for the third numerical simulation (according to Fig.5(c))

This fact can be more evident observing the Mach number distribution along the upper and lower frontiers of the field (see Fig. 11). Although very stable, the Mach number in the first part of the test section (before the model) had a uniform increase, starting from 0.181 (at the entrance) to 0.210 (one chord before the leading edge of the profile) – naturally this can be explained by the boundary-layer thickness-displacement growth along the superior wall. Note that the inferior frontier corresponds to the "centerline" of the wind tunnel and the Mach number was the same as observed in the tunnel wall at each longitudinal station in the first part of the test section. Here it is called "centerline" the line that represents the center of the test section, although in the region where the model is installed it really represents the line along the profile surface. It is also possible to observe small perturbations in the trailing edge region, which can be explained by the fact that the boundary-layer is abruptly extinct at the end of the profile, as it was considered in the

ISSN 2176-5480

present mathematical modeling. A more sophisticated approach could be implemented by some smoothness consideration in future researches.

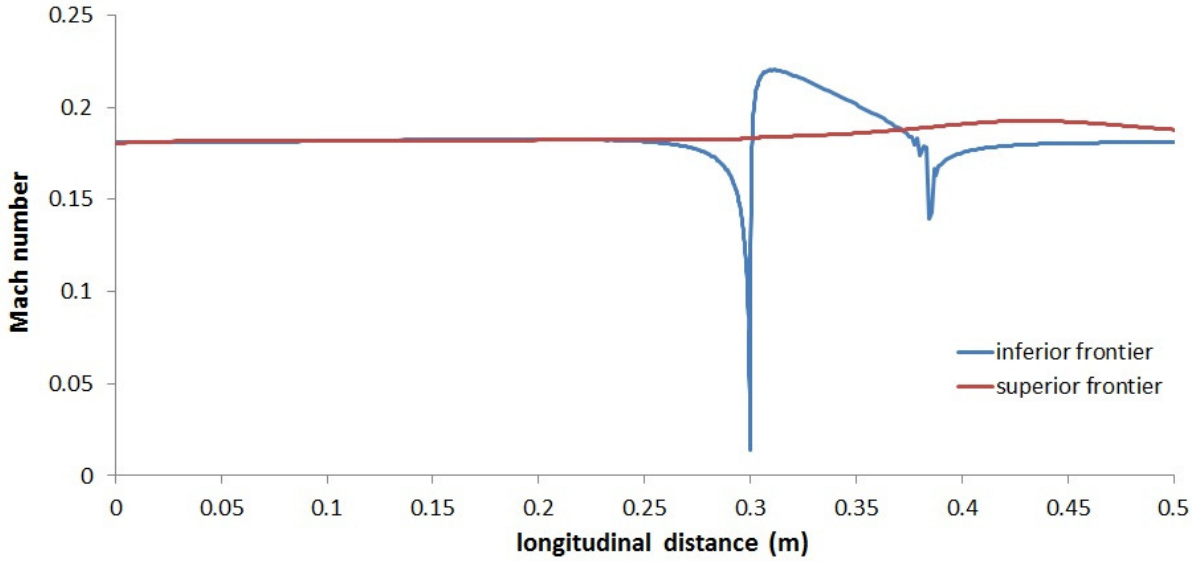

Figure 11. Mach number distributions in the inferior and superior frontiers of the calculation field – the inferior frontier corresponds to the wind tunnel longitudinal centerline

Figure 12 shows a comparison of the non-dimensional pressure distribution for all numerical cases studied. The pressure was made non-dimensional dividing it by the pressure value at the inlet section. It is important to say that for case 1, there is no upper wall and in this particular case the “upper wall” designation refers to the position where the wall would be, at the same position of case 2. Observe how small the maximum pressure disturbance in case 1 was: only about 0.1% of the total pressure level. In the real upper frontier of case 1, located at 3.6 chords from the tunnel centerline, no pressure disturbance could be observed, indicating that the boundary conditions (far field condition) in this line was well posed.

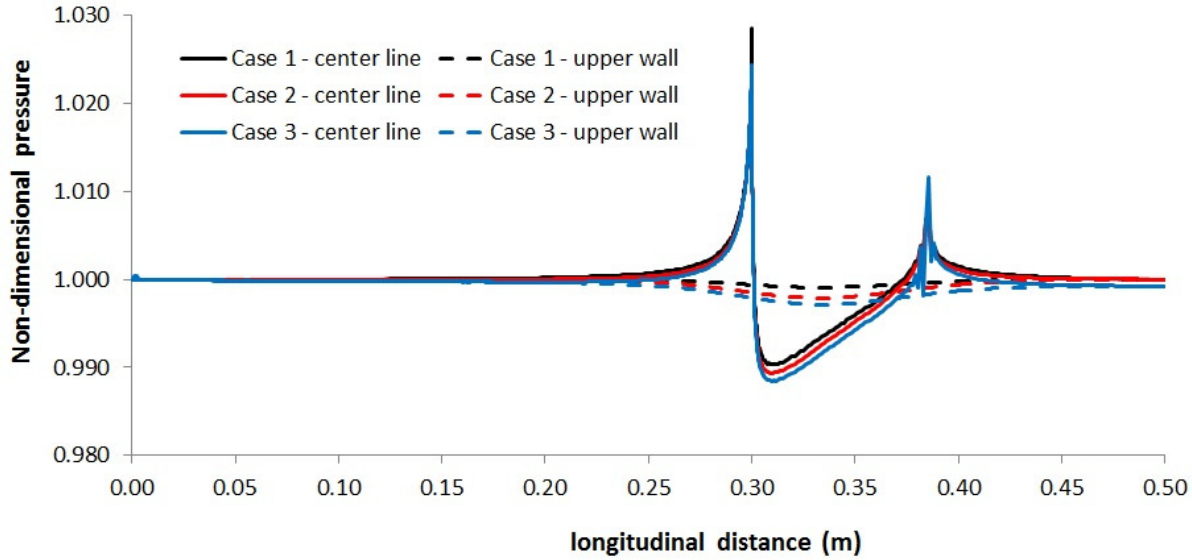

Figure 12. Non-dimensional pressure distribution in stream-wise direction for all cases at tunnel centerline (solid lines) and at the upper wall (dashed lines): the pressure is made non-dimensional in reference to the inlet section pressure

It is interesting to observe how the wall effects present in the field over-predict the pressure decrease on the profile surface, and consequently, on the upper wall. In other words, the wall reacts accordingly to the level of pressure on the

ISSN 2176-5480

model region. It is also worth of note that the Euler approach was not sufficient to account for the wall effects, as this was expected because of the real boundary-layer displacement-thickness growth along the solid frontiers. Again here one can observe the perturbation caused by the sudden vanishing of the boundary-layer on the profile surface, in the present simulation, as it was created by the mesh.

Figure 13 shows the *–Cp* distribution over the profile with results from experimental data, all three numerical simulation cases, freeware numerical simulation package Xfoil© (Drela and Youngren, 2012) and the experimental data corrected by the pressure loss observed in the tunnel test section according to Bredariol *et al.* (2012). The numerical simulation of the profile at free flight condition (case 1) was practically equivalent to the Xfoil© simulation, indicating that the boundary conditions adopted in the simulation were well posed. When the tunnel wall was considered in the numerical simulation, the *–Cp* distribution experienced stronger variations caused by the air flow acceleration between the model surface and the tunnel wall (case 2, red curve in Fig. 13). But this was not sufficient to reach the obtained experimental results (white diamond symbols in Fig. 13). When the boundary-layer displacement-thickness was included in the numerical simulation (case 3, blue curve in Fig. 13), the *–Cp* distribution had an even stronger variation caused by the same flow acceleration due to the air passage constriction. But still this was not sufficient to reach the experimental results obtained.

However, the relative long wind tunnel test section contributed to increase the pressure loss along its length provoking a considerable difference between the reference undisturbed pressure at the test section entrance and the pressure at the model installation local, as reported by Bredariol *et al.* (2012). If a correction of the reference undisturbed pressure at the test section entrance is made the corrected experimental results (black diamond symbol) have a very good agreement with the numerical simulation for the case 3 with boundary-layer consideration (blue curve).

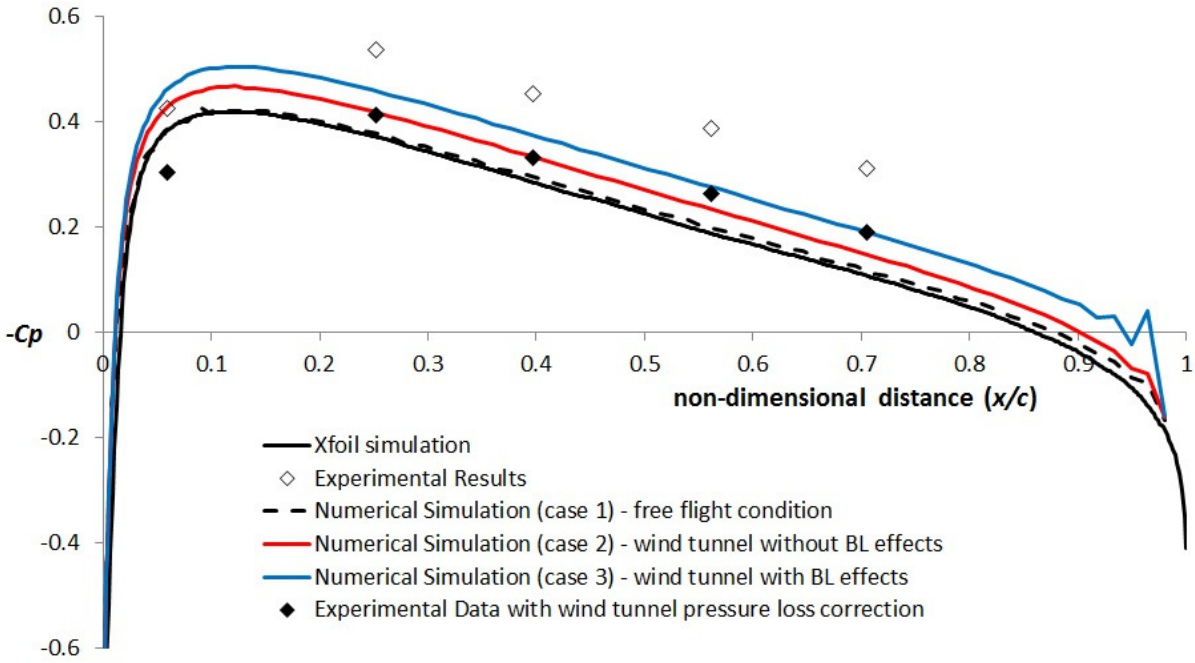

Figure 13. Distribution of *–Cp* along the profile chord (*c*) for experimental and numerical simulation cases

Nevertheless, there are still some points to observe. Comparing the experimental data with wind tunnel pressure loss correction with the numerical simulation with boundary-layer effects (case 3) the errors in terms of pressure and *–Cp* are shown in Table 2. The errors in the pressure coefficient (*–Cp*) indicate that along the chord it can have another important physical phenomenon that is not being corrected, and that makes the points close to the leading edge having a different behavior from the points close to the trailing edge. This is an important issue that will be considered in future investigations. Two initial ideas to be explored are the nature of the boundary layer over the profile, passing through a transition point between laminar and turbulent, and the induction effect caused by the proximity of the trailing edge to the mixing chamber entrance. The attention should be given also to the acquisition system, since the pressure scanner has a precision of 40 Pa and a better instrument is desirable to clarify the experimental results obtained.

Concerning the measured pressure values, the first experimental point calls the attention, being consistently lower than any of the tendency line of the numerical results. In future experiments this point will be thoroughly investigated to

ISSN 2176-5480

determine if there is some problem with the installation or if it is something related to the experimental procedure. This first point is very important as it is responsible for capturing the rise in the $-Cp$ curve.

Table 2. Relative discrepancies in $-C_P$ and pressure values between the experimental results corrected for the pressure loss in the wind tunnel and numerical simulation considering the boundary-layer effect (case 3) for the five experimental points

Experimental Point	Position (x/c)	Relative $-C_P$ error	Relative pressure error	Absolute pressure error
1	0.060	-35%	0.4%	333 Pa
2	0.252	-10%	0.1%	88 Pa
3	0.397	-10%	0.09%	86 Pa
4	0.562	-3%	0.02%	17 Pa
5	0.705	1%	0.00007%	6 Pa

5. CONCLUSION

A methodology based on numerical simulation was created and applied to the correction of the wall interference in a small subsonic wind tunnel of the Aerodynamic Division (ALA) of the Institute of Aeronautics and Space (IAE). The use of a very low computational cost code based on Euler equations proved to be unable of account for the boundary-layer effect when tested with a NACA 0012 profile installed in the test section. So the computational mesh was modified to reflect the boundary-layer displacement-thickness growth along the solid wall of the tunnel and the profile surface. The result was good when it was considered the tunnel pressure loss and the measured pressure values were corrected accordingly.

In future experiments special attention will be given to the first measuring point because after the correction applied the relative error in $-C_P$ was still very high (35%).

In general the points close to the leading edge have poor agreement after applying the correction methodology. This indicates that could exist some physical phenomenon still not predicted with this correction methodology and this will be the theme for further researches.

The use of numerical simulation for wall correction proved to be a useful and low cost tool.

6. ACKNOWLEDGEMENTS

The authors would like to express their gratitude to CNPq, the Brazilian Council of Research and Development by the help during the development of this work through grants 560200/2010-2 and 145121/2012-7.

7. REFERENCES

Anderson, J. D. Jr., 2007, *Fundamentals of Aerodynamics*, McGraw-Hill Higher Education, Boston, 4th Edition.

Barlow, J. B., Rae, W. H. Jr., Pope, A., 1999, *Low-Speed Wind Tunnel Testing*, John Wiley & Sons, New York, 3rd Edition.

Bredariol, A. F., Silva, A. R., Falcão Filho, J. B. P., 2012, "Analysis of a NACA 0012 Profile in a Small Subsonic Induction Driven Wind Tunnel," in Proceedings from 14th Brazilian Congress of Thermal Sciences and Engineering, ENCIT-2012.

Falcão Filho, J. B. P., Ortega, M. A., 2008, "Numerical Study of the Injection Process in a Transonic Wind Tunnel. The Numerical Details," Computers and Fluids, Vol. 37, Issue 10, December 2008, pp. 1276-1308, available online in: www.sciencedirect.com. DOI: 10.1016/j.compfluid.2007.10.015.

Faria, A. F., 2011,, "Desenvolvimento de uma Seção de Testes para um Mini Túnel de Vento", Trabalho de Graduação, Faculdade de Tecnologia São José dos Campos (FATEC).

Goffert, B., Truyts, C. F., Lima, D. S. A, Falcão Filho, J. B. P., 2008, "Control of Injection System for the Pilot Transonic Wind Tunnel of IAE in Closed Circuit", Proceedings ... XII Brazilian Congress of Thermal Engineering and Sciences, ENCIT-2008, Belo Horizonte-MG, article 1-5054.

Menezes, J. C. L., 1994, "Análise Numérica de Escoamentos Transônicos Turbulentos em Torno de Aerofólio," Tese de Mestrado, Instituto Tecnológico de Aeronáutica, São José dos Campos – SP.

PSI, 2000, "ESP-16BP Pressure Scanner User´s Manual," catalog of products of Esterline Pressure Systems 3rd Edition – www.pressuresystems.com.

ISSN 2176-5480

Pulliam, T. H., 1986, "Artificial Dissipation Models for the Euler Equations," *AIAA Journal*, 24(12), pp. 1931-1940.
Pulliam, T. H., Chaussee, D. S., 1981, "A Diagonal Form of an Implicit Approximate-Factorization Algorithm. *Journal of Computer Physics*, 1981; 39: 347-363.
Silva, A. F. C., Ortega, M. A., Falcão Filho, J. B. P., 2010, "Diffuser Design for a Supersonic/Subsonic Mixing Chamber," Proceedings from 13rd Brazilian Congress of Thermal Sciences and Engineering, Dec. 05-10, Uberlândia, Minas Gerais, Brasil.
Silva, A. F. C., Ortega, M. A., Nogueira, S. L., Falcão Filho, J. B. P., 2010, "Supersonic Injector Design for Using in a Mixing Chamber," Proceedings from 13rd Brazilian Congress of Thermal Sciences and Engineering, Dec. 05-10, Uberlândia, Minas Gerais, Brasil.
Silva, A. F. C., Godinho, M. B. C., Ortega, M. A., Falcão Filho, J. B. P., 2011, "Supersonic/Subsonic Mixing Chamber Experimental Analysis," proceedings from 21st Brazilian Congress of Mechanical Engineering, Natal, RN, Brazil.

8. RESPONSIBILITY NOTICE

The authors are the only responsible for the printed material included in this paper.